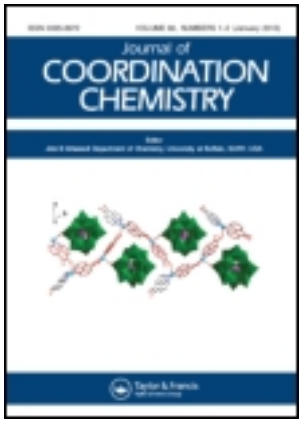

Journal of Coordination Chemistry
Publication details, including instructions for authors and subscription information:
http://www.tandfonline.com/loi/gcoo20

Two metal-pipemidic acid complexes modifying Keggin polyoxometalates

Jingquan Sha [a], Taoye Zheng [a], Erlin Zhang [a], Hongbin Qiu [a], MINGYUAN LIU [a], HONG ZHAO [a] & HUAN YUAN [a]

[a] The Provincial Key Laboratory of Biological Medicine Formulation, School of Pharmacy, Jiamusi University, Jiamusi, PR China

Accepted author version posted online: 11 Feb 2013.Published online: 20 Mar 2013.

To cite this article: Jingquan Sha, Taoye Zheng, Erlin Zhang, Hongbin Qiu, MINGYUAN LIU, HONG ZHAO & HUAN YUAN (2013) Two metal-pipemidic acid complexes modifying Keggin polyoxometalates, Journal of Coordination Chemistry, 66:6, 977-985, DOI: 10.1080/00958972.2013.774387

To link to this article: http://dx.doi.org/10.1080/00958972.2013.774387

Journal of Coordination Chemistry
Vol. 66, No. 6, 20 March 2013, 977–985

Two metal-pipemidic acid complexes modifying Keggin polyoxometalates

JINGQUAN SHA, TAOYE ZHENG, ERLIN ZHANG, HONGBIN QIU*, MINGYUAN LIU, HONG ZHAO and HUAN YUAN

The Provincial Key Laboratory of Biological Medicine Formulation, School of Pharmacy, Jiamusi University, Jiamusi, PR China

(*Received 11 June 2012; in final form 4 December 2012*)

Two new organic–inorganic hybrid compounds based on Keggin polyoxometalates (POMs) and the quinolone antibacterial, pipemidic acid (HPPA), $\{[Cu(PPA)_2]_2[H_3PMo_{12}O_{40}]\}\cdot 8H_2O$ (**1**), and $\{[Zn(PPA)_2][H_3PMo_{12}O_{40}]\}\cdot[HPPA]\cdot 3H_2O$ (**2**) have been synthesized under hydrothermal conditions and structurally characterized. In **1**, Keggin POMs combine with two chelate $Cu(PPA)_2$ complexes forming a discrete "seesaw-like" motif, while Keggin POMs combine with the binuclear zinc clusters $[Zn_2(PPA)_4]$ forming a discrete "dumbbell-like" motif in **2**. Antitumor activities *in vitro* and the interactions with CT-DNA of the compounds have been investigated by MTT experiment and UV spectra, respectively.

Keywords: Polyoxometalate; Pipemidic acid; Antitumor activity; Interaction with CT-DNA

1. Introduction

Polyoxometalates (POMs), as early transition metal oxide clusters, are an appealing area in organic–inorganic hybrid chemistry because of their versatile structures and potential applications in catalysis, materials science, magnetism, and medicine [1–5]. One of the most intriguing areas is the development of inorganic–organic hybrids-based POMs for medical applications. This field is in its infancy, but first approaches are reported, such as amino acid-functionalized POMs [6, 7], fluorouracil-containing $[BW_{12}O_{40}]^{5-}$ [8], surfactant, and dendritic encapsulated clusters, as well as starch and liposome encapsulated POMs [9, 10].

When summarizing applications of POMs in medicine, the main problems that prevent application of POMs in medicine are low-hydrolytic stability and, in particular, low selectivity (accumulation in the reticuloendothelial system). Toxicity of POMs is strongly dependent on the structure, with low-toxic POMs ($[SiW_{12}O_{40}]^{4-}$, $[PW_{12}O_{40}]^{3-}$) and high-toxic compounds, such as HPA-23 [11]. Modification of POMs is a promising route [6–10, 12–14] for the following reasons: (1) nearly every molecular property that impacts the recognition and reactivity of POMs with target biological macromolecules can be altered easily, such as polarity, redox, surface charge distribution, shape, and acidity; (2) the surface of POMs can be modified to enable the design of multifunctional compounds by covalent

*Corresponding author. Email: jdzhiyao@163.com

ISSN 0095-8972 print/ISSN 1029-0389 online
http://dx.doi.org/10.1080/00958972.2013.774387

attachment of organic groups; (3) study of the interaction between drugs and transition metals is also an important research area in bioinorganic chemistry [15–17]. Action of many drugs is dependent on coordination with metal ions [15] and/or the inhibition [16] on the formation of metalloenzymes. Therefore, metal ions might play vital roles during the drug utilization in the body.

During our efforts to modify and functionalize POMs with biological active molecules [18], pipemidic acid (HPPA), a second-generation quinolone antimicrobial drug, has captured our attention because HPPA is an antibacterial drug and also an excellent multidentate ligand coordinating with metal ions to further modify POMs. Our group has reported several multifunctional hybrid compounds based on Keggin POMs and quinolone drugs [18, 19]. As an ongoing effort, in this work we obtained two Cu/Zn–PPA complexes modifying Keggin POMs, $\{[Cu(PPA)_2]_2[H_3PMo_{12}O_{40}]\}\cdot 8H_2O$ (**1**), and $\{[Zn(PPA)_2][H_3PMo_{12}O_{40}]\}\cdot[HPPA]\cdot 3H_2O$ (**2**). To explore the properties of hybrid compounds, the antitumor activities *in vitro* and the interactions of the compounds with CT-DNA have been investigated by MTT experiment and UV spectra, respectively.

2. Experimental

2.1. *Materials and methods*

All reagents were purchased commercially and used without purification. DNA stock solution was prepared by dilution of CT-DNA to buffer solution (50 mL 0.1 ML^{-1} tris solution and 42 mL 0.1 ML^{-1} hydrochloric acid, diluted to 100 mL), followed by exhaustive stirring at 4 °C for three days, and kept at 4 °C for no longer than a week. The stock solution of CT-DNA gave a ratio of UV absorbance at 260 and 280 nm (A260/A280) of 1.90 indicating that the DNA was sufficiently free of protein contamination. DNA concentration was determined by the UV absorbance at 260 nm after 1 : 20 dilution using $\varepsilon = 6600\ M^{-1}\ cm^{-1}$. Elemental analyses were performed on a Perkin-Elmer 2400 CHN Elemental Analyzer (C, H, and N) and a Leaman inductively coupled plasma spectrometer (Cu and Zn). IR spectra on KBr pellets were recorded on a Nicolet 170SX FTIR spectrophotometer from 400–4000 cm^{-1}. UV–Visible (UV–Vis) spectra were recorded in a UV-2550. TG analyses were performed on a Perkin-Elmer TGA7 instrument with a heating rate of 10 °C min^{-1}. The XRPD patterns were obtained with a Rigaku D/max 2500 V PC diffractometer with Cu-Kα radiation, the scanning rate is 4°/s, 2θ ranging from 4–50°.

2.2. *Syntheses*

2.2.1. $\{[Cu(PPA)_2]_2[H_3PMo_{12}O_{40}]\}\cdot 8H_2O$ (1). A mixture of $H_3[PMo_{12}O_{40}]$ (300 mg), $Cu(CH_3COO)_2\cdot H_2O$ (50 mg), HPPA (60 mg), $NaHCO_3$ (20 mg), and H_2O (10 mL) was stirred for 1 h in air. The pH was then adjusted to *ca.* 4.0 with 1 M CH_3COOH and the mixture was transferred to a 20 ml Teflon-lined reactor. After heating at 155 °C for six days, the reactor was slowly cooled to room temperature. Purplish blue block crystals of **1** were filtered, washed with water, and dried at room temperature. $PMo_{12}O_{60}Cu_2C_{56}N_{20}H_{83}$ (3305): Calcd C, 20.33; H, 2.51; N, 8.47; Cu, 3.87%. Found: C, 20.26; H, 2.61; N, 8.46; Cu, 3.85%.

2.2.2. {[Zn(PPA)$_2$][H$_3$PMo$_{12}$O$_{40}$]}·[HPPA]·3H$_2$O (2). Compound **2** was prepared in a manner similar to that described for **1**, except the $Zn(CH_3COO)_2$ replaced $Cu(CH_3COO)_2$. Light gray block crystals were obtained. $PMo_{12}O_{52}ZnC_{42}N_{15}H_{58}$ (2852): Calcd C, 17.67; H, 2.03; N, 7.36; Zn, 2.29%. Found: C, 17.62; H, 2.08; N, 7.34; Zn, 2.25%.

2.3. *X-ray crystallographic study*

Crystal data for **1** and **2** were collected on a Bruker SMART-CCD diffractometer with Mo-Kα monochromatic radiation ($\lambda = 0.71069$ Å) at 293 K. All structures were solved by direct methods and refined by full-matrix least-squares on F^2 using the SHELXTL crystallographic software package [20]. All non-hydrogen atoms were refined anisotropically. The positions of hydrogens on carbon were calculated theoretically. The crystal data and structure refinements of **1** and **2** are summarized in table 1. Selected bond lengths and angles for **1** and **2** are listed in tables S1 and S2.

2.4. *DNA binding studies*

Study of the interaction of complexes with DNA is of great importance since their activities as antibacterial drugs are focused on inhibition of DNA replication [21]. DNA can provide three distinctive binding sites for quinolone metal complexes (groove binding, electrostatic binding to phosphate, and intercalation) [22]. The interaction can be studied with UV spectroscopy to determine the possible binding modes to CT-DNA. Changes observed in UV spectra upon titration may give evidence of the interaction mode, since a hypochromism, due to π–π^* stacking interactions, may appear in the case of intercalative

Table 1. Selected crystallographic data for **1** and **2**.[a,b]

Compounds	**1**	**2**
Empirical formula	$PMo_{12}O_{56}Cu_2C_{56}N_{20}H_{75}$	$PMo_{12}O_{52}ZnC_{42}N_{15}H_{58}$
Mr	3305	2852
CCDC	837119	837120
Crystal system	Monolinic	Triclinic
Space group	*P21/c*	*P−1*
Theta range for data collection	1.46°–25.00°	1.10°–28.29°
a, Å	12.470(5)	12.723(5)
b, Å	22.398(5)	17.224(5)
c, Å	17.832(5)	19.259(5)
α, deg	90.000(5)	103.611(5)
β, deg	90.310(5)	92.580(5)
γ, deg	90.000(5)	110.293(5)
V, Å^3	4981(3)	3810(2)
Z	2	2
D_{calcd}, g cm^{-3}	2.194	2.481
F(000), *e*	3202	2748
Reflections collected/unique	24538/8768 [*R*(int) = 0.1951]	23845/17408 [*R*(int) = 0.0270]
Completeness to theta = 25.00	99.8%	99.3%
R_1/wR_2 [$I > 2\sigma(I)$]	0.0824, 0.1921	0.0504, 0.1204
GoF (F^2)	0.959	1.021

[a] $R_1 = \sum ||F_0| - |F_c|| / \sum |F_0|$.

[b] $wR_2 = \sum [w(F_0^2 - F_c^2)^2] / \sum [w(F_0^2)^2]^{\frac{1}{2}}$.

binding, while red-shift (bathochromism) may be observed when the DNA duplex is stabilized. In UV titration experiments, the spectra of CT-DNA in the presence of each compound were recorded for a constant CT-DNA concentration in different [complex]/[CT-DNA] mixing ratios (r).

2.5. *Antitumor activity studies*

The antitumor activity of **1** and **2** and their parent anion on SGC7901 cells was tested by the MTT (abbreviation 3-[4,5-dimethylthiazol-2-yl]-2.5-diphenyltetrazolium bromide) experiment [23]. Subcultured SGC7901 cells were suspended in 0.25% trypsin. The cell suspension (*ca.* 10^5–10^6 cells mL) was added to a 96 well plate (100 μL per well) and incubated at 37 °C in a 5% CO_2 incubator for 24 h. Samples (100 μL) containing the compounds were then added. After 48 h, 20 μL MTT solution (5 mg ML^{-1} in 0.01 M PBS (phosphate buffer solution)) was added and the mixture was incubated for 4 h. The supernatant was removed and DMSO (150 μL) was added. The resulting mixture was shaken for 10 min at room temperature and colorimetric analysis was used to examine the cell survival rate. These samples containing **1**, **2**, and parent compound were obtained by dissolving in DMSO, autoclaving, and diluting by a RPMI 1640 medium to a final concentration of 100, 50, 25, 12.5, and 6.25 μg mL^{-1}.

3. Results and discussion

3.1. *Crystal structures*

3.1.1. Structure description of 1. Single crystal X-ray structural analysis reveals that **1** is composed of one $[PMo_{12}O_{40}]^{3-}$ (abbreviated to $\{PMo_{12}\}$), two $[Cu(PPA)_2]^{2+}$, and eight waters (figure 1(a)). In the compound, $\{PMo_{12}\}$ is the classical α-Keggin type. The bond lengths and angles are in the normal range except for a disordered $[PO_4]^{3-}$ in the center. Valence sum calculations [24] show that all Mo are in the +6 oxidation state and Cu are in the +2 oxidation states. Each $\{PMo_{12}\}$ polyoxoanion is a bidentate inorganic ligand coordinating with two Cu^{2+} ions through two terminal oxygens. The Cu^{2+} is square pyramidal, achieved by one oxygen from $\{PMo_{12}\}$ and four oxygens from two PPA ligands. The corresponding bond lengths are 2.485 Å for $Cu1O_{POM}$ and 1.897–1.956 Å for $Cu1O_{PPA}$. PPA adopts chelate coordination. As a result, **1** shows a discrete "seesaw-like" motif. Intermolecular interactions play vital roles in stabilizing the structure of **1**. For example, adjacent "seesaw-like" subunits connect forming 1-D chains through short interaction with O28 ⋯ N6 (2.678 Å), O25 ⋯ N1 (2.776 Å), and O17 ⋯ N1 (2.866 Å) as shown in figure 1(b). There are extensive π ⋯ π interactions among organic ligands, which result in adjacent $\{[Cu(PPA)_2]_2[PMo_{12}O_{40}]\}_n$ chains forming a 2-D layer and the centroid⋯centroid distance between two adjacent aryl rings is *ca.* 3.7 Å, shown in figure 1(c) and figure 1(d). Intermolecular interactions connect neighboring 2-D layers to form a supramolecular 3-D structure (figure 1(e)).

3.1.2. Structure description of 2. Single crystal X-ray structural analysis reveals that **2** is constructed from one PMo_{12}, one $[Zn(PPA)_2]^{2+}$, one isolated HPPA, and three waters (figure 2(a)). The parent PMo_{12} is similar to **1**, except for having ordered $[PO_4]^{3-}$ in the center. The valence sum calculations show that all the Mo are +6 and Zn are +2. The one

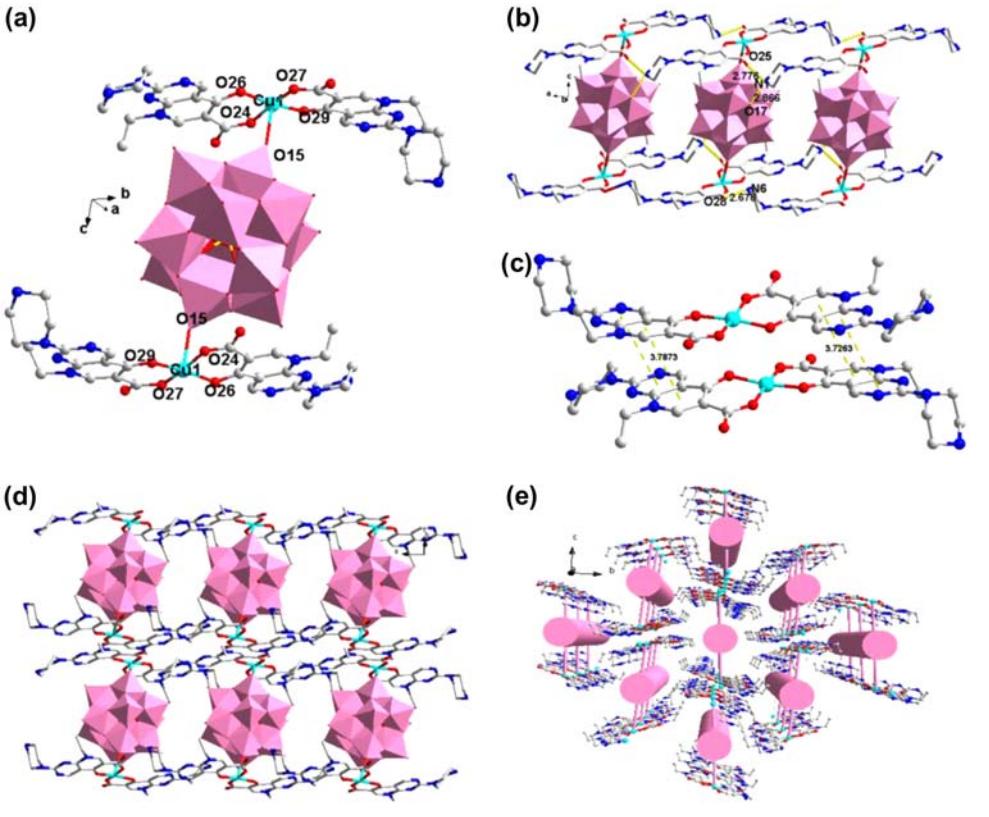

Figure 1. (a) Fundamental building block of **1**. Only some atoms are labeled; water molecules and all hydrogens are omitted for clarity. (b) Supramolecular organic–inorganic hybrid chains based on POMs and PPA. (c) The interactions between two adjacent aryl rings. (d) 2-D layer and (e) 3-D structure constructed by {[Cu$(PPA)_2]_2[PMo_{12}O_{40}]$} subunits.

crystallographically independent zinc (Zn1) is six-coordinate by five O from three PPA and one O from PMo_{12} in octahedral coordination. The bond distances around Zn1 are 2.288 Å for $Zn1O_{POM}$ and 1.957 – 2.124 Å for $Zn1\text{-}O_{PPA}$. Two crystallographically unique PPA molecules exhibit different roles, one as bridging and chelating tri-dentate ligands and another as chelating bidentate covalently linking to the same two zinc ions forming the binuclear zinc (figure 2(b)). Note that O3 W connects adjacent {$[Zn(PPA)_2][PMo_{12}O_{40}]$} subunits forming "peanut-like" chains via O33 and O18 (figure 2(c)). Isolated water and HPPA molecules donate different kinds of hydrogen bonds stabilizing the whole structure; as a result the ultimate supramolecular 3-D structure is formed (figure 2(d)).

3.2. *FTIR spectra, TG analyses, and XRPD characterization*

The XRPD patterns for **1** and **2** are presented in figures S1 and S2. The diffraction peaks of both simulated and experimental patterns match well indicating that the phase purities of the **1** and **2** are good. The difference in reflection intensities between the simulated and the experimental patterns is due to the different orientation of the crystals in the powder samples. In IR spectra (figures S3 and S4), characteristic peaks at 1055, 952, 874, 787 cm^{-1} for

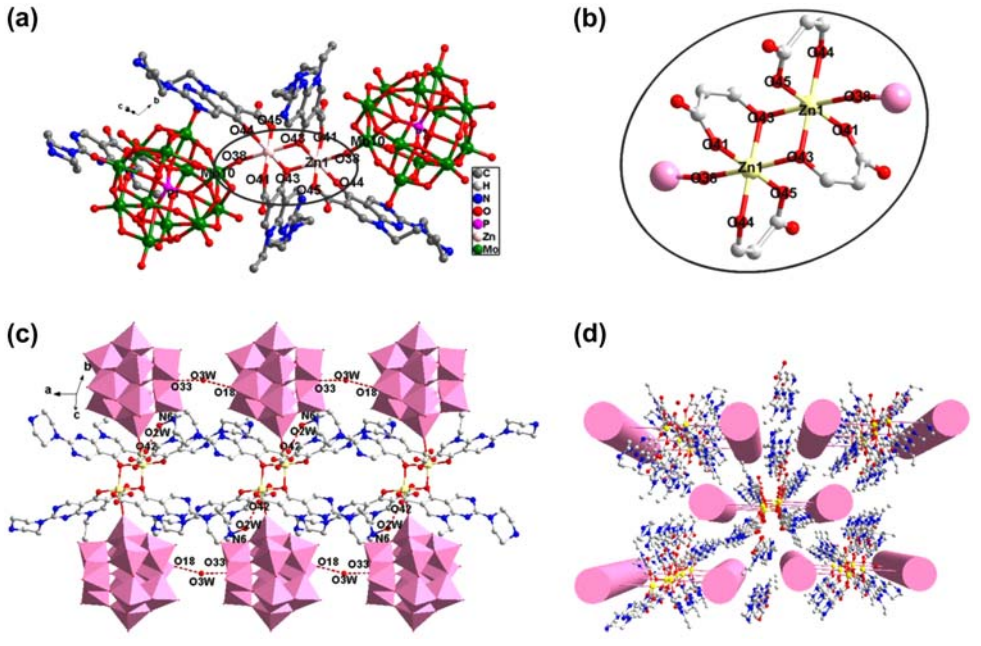

Figure 2. (a) Fundamental building block of **2**. Only some atoms are labeled and waters and all hydrogens are omitted for clarity. (b) The binuclear zinc cluster. (c) "Peanut-like" supramolecular organic–inorganic hybrid chains based on $\{[Zn(PPA)_2][PMo_{12}O_{40}]\}$ subunits. (d) The 3-D structure of **2**.

1 and 1057, 955, 864, 796 cm^{-1} for **2** are attributed to ν_{as}(P–O), ν_{as}(Mo–Od), ν_{as}(Mo–Ob–Mo), and ν_{as}(Mo–Oc–Mo), which are nearly identical to those of $[PMo_{12}O_{40}]^{3-}$ (figure S5) except for slight changes in peak position, perhaps due to coordination. Furthermore, bands at 1620–1200 cm^{-1} can be attributed to HPPA molecules. To characterize the thermal stabilities, their thermal behaviors were studied by TG analyses (figure S6). The experiment was performed on crystalline samples under air. For **1**, thermal analysis gives a total loss of 40.98% from 30–520 °C, which agrees with the calculated weight loss of 41.02%: the first weight loss of 4.33% at 30–208 °C corresponds to loss of eight waters per formula (calcd 4.35%) and the second continuous weight loss of 36.65% at 208–520 °C arises from decomposition of PPA (calcd 36.67%). For **2**, the first weight loss of 1.89 at 30–220 °C corresponds to loss of three molecules per formula (calc. 1.89%) and the second continuous weight loss of 31.82% at 220–550 °C arises from decomposition of PPA (calcd 31.87%). The results also support the chemical compositions of **1** and **2**.

3.3. *Interaction with DNA*

UV spectra of CT-DNA in the presence of HPPA as well as **1** and **2** have been recorded for different [compound]/[DNA] mixing ratios (r) shown in figure 3. The changes observed in the absorption spectra, namely, the increase of the intensity at $\lambda_{max} = 258$ nm accompanied with a red-shift of the λ_{max} to 260 nm for HPPA and **1**, and 263 nm for **2**, after mixing with each compound, indicate that the interaction with CT-DNA results in formation of a new compound [25]. The absorption intensity at 258 nm is increased due to the fact that the purine and pyrimidine DNA-bases are exposed because of the binding of the

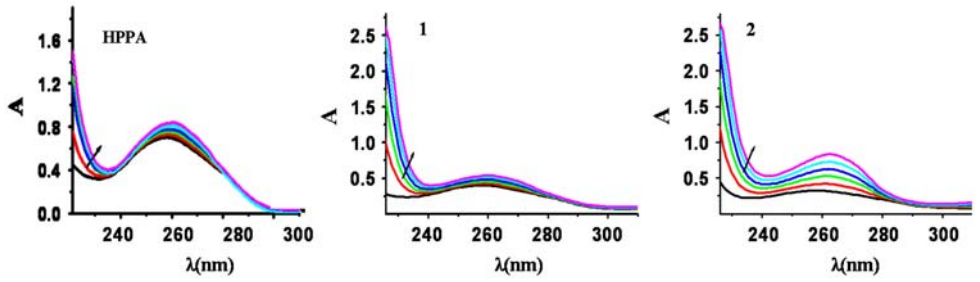

Figure 3. UV spectra of CT-DNA in buffer solution in the absence or presence of HPPA ([DNA] = 1×10^{-5} M), **1** ([DNA] = 6×10^{-5} M) and **2** ([DNA] = 4.8×10^{-5} M). The arrows show the changes upon increasing amounts of compounds.

compounds to DNA. These characteristics can be attributed to an interaction having caused changes of the conformation of DNA [26]. The observed red-shift (bathochromism) is evidence of stabilization of the CT-DNA duplex, while the existence of the intercalative binding mode may not be ruled out [27].

In figure 4, changes occurred in the spectra of a 10^{-5} M solution of HPPA, **1** and **2** during the titration upon addition of CT-DNA with different r values presented. In the UV region, intense absorptions observed in spectra of the quinolones and **1** and **2** are attributed to intra-ligand π–π* transition of the coordinated groups [28]. Any interaction between each compound and CT-DNA could perturb the intra-ligand centered spectral transition bands of the complex. As shown in figure 4, bands centered at 355 nm exhibit hypochromism for HPPA in the presence of increasing amounts of CT-DNA; at 331 nm a hypochromism for **1**, at 332 nm a hypochromism for **2**. The resultant hypochromism suggests tight binding of compounds to CT-DNA, probably by intercalation. So the above discussed results suggest that the compounds bind to CT-DNA and stabilize the DNA duplex.

As a tool investigating the magnitude of the binding strength with CT-DNA, the intrinsic binding constant K_b can be obtained by monitoring changes in the absorbance at the corresponding λ_{max} with increasing concentrations of CT-DNA from plots $\frac{[DNA]}{(\varepsilon_a - \varepsilon_f)}$ *vs.* [DNA] (inset of figure 4) and is given by the ratio of slope to the y intercept, according to the following equation [29]:

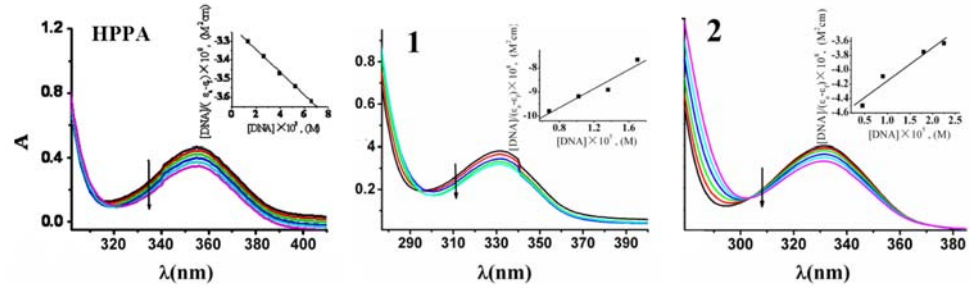

Figure 4. UV spectra of HPPA (5×10^{-5} M), **1** (7×10^{-5} M), and **2** (5×10^{-5} M) in DMSO solution in the presence of CT-DNA at increasing amounts. The arrows show the changes upon increasing amounts of CT-DNA. Insets: plots of $[DNA]/(\varepsilon_a - \varepsilon_f)$ *vs.* [DNA].

$$\frac{[DNA]}{(\varepsilon_a - \varepsilon_f)} = \frac{[DNA]}{(\varepsilon_b - \varepsilon_f)} + \frac{1}{K_b(\varepsilon_b - \varepsilon_f)} \quad (1)$$

where $\varepsilon_a = A_{obsd}/[(compound)]$, ε_f = extinction coefficient for the free compound, and ε_b = extinction coefficient for the compound in the fully bound form.

The calculated K_b values for HPPA, **1**, and **2** are $1.88(\pm0.02) \times 10^3\,M^{-1}$, $1.76(\pm0.02)$, and $1.00(\pm0.06) \times 10^4\,M^{-1}$, respectively, which suggest moderate binding of each compound to CT-DNA. Note that the K_b values of **1** and **2** are much higher than their parent drugs, indicating that the coordinated "seesaw-like" in **1** and the "dumbbell-like" in **2** POM-TM-PPA subunits can change the configuration of drugs, and the resulted configurations favor interaction with CT-DNA.

3.4. *Antitumor activity studies*

A comparison of the antitumor activity for **1** and **2** and their parent PMo_{12} was made (see table S3). The inhibitory effect against SGC7901 lines shows that the parent PMo_{12} exhibits higher antitumor activity to SGC7901 and the values of the inhibitory cell 50% lethal concentration (IC_{50}) are 0.078 mg/ml, while the two new compounds show no anti-SGC7901 activities. This indicates that introduction of metal complexes of HPPA onto the PMo_{12} polyoxoanion surface may decrease antitumor activity. Although the result is different from the reported results [15, 16], combining with the actual and reported results, we can draw conclusions that the antitumor activity of POMs may be modulated by the metal-organic subunits.

4. Conclusions

Based on our previous work, we investigated TM-PPA complexes modifying PMo_{12}, and two new TM-PPA-PMo_{12} compounds have been obtained. UV studies of the interaction of compounds with CT-DNA show that the new compounds bind to CT-DNA and exhibit higher binding constant to CT-DNA than their parent drugs. The MTT investigations find that the antitumor activities of PMo_{12} are higher than that of the two new compounds, different from the reported results, but we draw conclusions that the antitumor activities of POMs-based compounds may be modulated by metal-organic subunits. So their isolation is helpful to extend the applications of POMs in medicine; more work needs to be done about TM-drugs-POMs reaction systems to explore the possible effect of drug molecules modifying POM clusters.

Supplementary data

Crystallographic data and CCDC can be obtained free of charge from the Cambridge Crystallographic Data Center via www.ccdc.cam.ac.uk/data_request/cif. Tables of selected bond lengths (Å), bond angles (°), and IR for compounds are provided in supporting information.

Acknowledgments

This work is financially supported by the National Natural Science Foundation (Grant Nos. 20901031 and 21271089) and Scientific and technological innovation team (2012TD010)

and Scientific and technological project (GC09C317), and Postdoctoral Foundation of Heilongjiang Province.

References

[1] D.L. Long, E. Burkholder, L. Cronin. *Chem. Soc. Rev.*, **36**, 105 (2007).
[2] P.P. Mishra, J. Pigga, T.B. Liu. *J. Am. Chem. Soc.*, **130**, 1548 (2008).
[3] S.D. Jiang, B.W. Wang, G. Su, Z.M. Wang, S. Gao. *Angew. Chem. Int. Ed.*, **10**, 1736 (2010).
[4] T. Ishida, M. Nagaoka, T. Akita, M. Haruta. *Chem. Eur. J.*, **14**, 8456 (2008).
[5] X. Wang, J. Liu, M.T. Pope. *Dalton Trans.*, **957**, (2003).
[6] J. Li, Y.F. Qi, J. Li. *J. Coord. Chem.*, **57**, 1309 (2005).
[7] H. Zhang, Y. Lan, L.Y. Duan. *J. Coord. Chem.*, **56**, 85 (2003).
[8] J. Li, J. Li, Y.F. Qi, H.F. Wang, E.B. Wang, C.W. Hu, L. Xu, X.Y. Wu. *Chem. J. Chin. Univ.*, **25**, 1010 (2004).
[9] W.F. Bu, L.X. Wu, X. Zhang, A.C. Tang. *J. Phys. Chem. B*, **107**, 13425 (2003).
[10] H.Y. An, D.R. Xiao, E.B. Wang, C.Y. Sun, Y.G. Li, L. Xu. *J. Mol. Struct.*, **751**, 184 (2005).
[11] W. Rozenbaum, D. Dormont, B. Spire, E. Vilmer, M. Gentilini, L. Montagnier, F.B. Sinoussi, J.C. Chermann. *Lancet*, **450**, (1985).
[12] A.X. Tian, X.L. Lin, Y.J. Liu, G.Y. Liu, J. Ying, X.L. Wang, H.Y. Lin. *J. Coord. Chem.*, **65**, 2147 (2012).
[13] M.L. Wei, H.H. Li, G.J. He. *J. Coord. Chem.*, **64**, 4318 (2011).
[14] P. Shringarpure, B.K. Tripuramallu, K. Patel, A. Patel. *J. Coord. Chem.*, **64**, 4016 (2011).
[15] A. Albert. *The Physico-Chemical Basis of Therapy: Selective Toxicity*, 6th Edn. Edn, Chapman & Hall, London (1979).
[16] M.N. Hughes (Ed.). *The Inorganic Chemistry of Biological Processes*, Wiley, New York, NY (1981).
[17] M. Patel, D. Gandhi, P. Parmar. *J. Coord. Chem.*, **64**, 1276 (2011).
[18] J.Q. Sha, L.Y. Liang, X. Li, Y. Zhang, H. Yan, G. Chen. *Polyhedron*, **30**, 1657 (2011).
[19] J.Q. Sha, L.Y. Liang, P.F. Yan, G.M. Li, C. Wang, D.Y. Ma. *Polyhedron*, **31**, 422 (2012).
[20] (a) G.M. Sheldrick. *SHELX-97, Program for Crystal Structure Refinement*, University of Gottingen, Germany (1997); (b) G.M. Sheldrick. *SHELXL-97, Program for Crystal Structure Solution*, University of Gottingen, Germany (1997).
[21] D.E. King, R. Malone, S.H. Lilley. *Am. Fam. Physician*, **61**, 2741 (2000).
[22] B.M. Zeglis, V.C. Pierre, J.K. Barton. *Chem. Commun.*, **4565**, (2007).
[23] X.H. Wang, J.F. Liu, Y.G. Chen, Q. Liu, J.T. Liu, M.T. Pope. *J. Chem. Soc., Dalton Trans.*, **1139**, (2000).
[24] I.D. Brown, D. Altermatt. *Acta. Crystallogr. Sect. B*, **41**, 244 (1985).
[25] Q. Zhang, J. Liu, H. Chao, G. Xue, L. Ji. *J. Inorg. Biochem.*, **83**, 49 (2001).
[26] Y.M. Song, Q. Wu, P.J. Yang, N.N. Luan, L.F. Wang, Y.M. Liu. *J. Inorg. Biochem.*, **100**, 1685 (2006).
[27] E.K. Efthimiadou, M. Katsarou, Y. Sanakis, C.P. Raptopoulou, A. Karaliota, N. Katsaros, G. Psomas. *J. Inorg. Biochem.*, **100**, 1378 (2006).
[28] G. Pratviel, J. Bernadou, B. Meunier. *Adv. Inorg. Chem.*, **45**, 251 (1998).
[29] A.M. Pyle, J.P. Rehmann, R. Meshoyrer, C.V. Kumar, N.J. Turro, J.K. Barton. *J. Am. Chem. Soc.*, **111**, 3053 (1989).